Unraveling intermittent features in single-particle trajectories by a local convex hull method

Yann Lanoiselée[*]
Laboratoire de Physique de la Matière Condensée (UMR 7643), CNRS–Ecole Polytechnique, University Paris-Saclay, 91128 Palaiseau, France

Denis S. Grebenkov[†]
Laboratoire de Physique de la Matière Condensée (UMR 7643), CNRS–Ecole Polytechnique, University Paris-Saclay, 91128 Palaiseau, France
and Interdisciplinary Scientific Center Poncelet (ISCP), Bolshoy Vlasyevskiy Pereulok 11, 119002 Moscow, Russia
(Received 6 April 2017; revised manuscript received 19 July 2017; published 22 August 2017)

We propose a model-free method to detect change points between distinct phases in a single random trajectory of an intermittent stochastic process. The local convex hull (LCH) is constructed for each trajectory point, while its geometric properties (e.g., the diameter or the volume) are used as discriminators between phases. The efficiency of the LCH method is validated for six models of intermittent motion, including Brownian motion with different diffusivities or drifts, fractional Brownian motion with different Hurst exponents, and surface-mediated diffusion. We discuss potential applications of the method for detection of active and passive phases in the intracellular transport, temporal trapping or binding of diffusing molecules, alternating bulk and surface diffusion, run and tumble (or search) phases in the motion of bacteria and foraging animals, and instantaneous firing rates in neurons.

DOI: 10.1103/PhysRevE.96.022144

I. INTRODUCTION

Identifying transport mechanisms in complex systems and building their mathematical models is a challenging problem of paramount importance, especially in microbiology. While numerous experimental observations clearly revealed anomalous diffusion features in the intracellular transport, their microscopic biophysical origins remain debatable [1–9]. The significant technological progress in optical microscopy over the past decade has opened new opportunities in the statistical analysis of single particle trajectories but also raised challenges in the biophysical interpretation of a small number of random trajectories. Most theoretical works remain focused on the simplest observable, the time-averaged mean-square displacement (TA MSD), which has been studied for many anomalous diffusion models (see Refs. [10–12] and references therein). However, since this observable does not discriminate between various models, other observables have been proposed, e.g., first passage times [13,14], the maximum excursion [15], fundamental moments [16], and the fractal dimension of the explored space [17] (see also Ref. [18] and references therein). At the level of a single trajectory, elaborate statistical tools have been developed to recognize fractional Brownian motion (fBm) [19], to distinguish between fBm and continuous time random walk (CTRW) [20–22], and to reveal ergodicity breaking [23,24]. In addition, various statistical tests from econometric studies can be employed in the biophysical context, e.g., testing the Markov hypothesis [25]. Once an appropriate model of anomalous diffusion is identified, one can estimate its parameters that are related to the intracellular transport and then rely on the theoretical knowledge about the model to predict biological implications, e.g., biochemical reaction rates, translocation or transcription mechanisms, drug delivery, etc. [9,26].

The advantages of conventional models such as fBm or CTRW are the reduced number of model parameters and a possibility to describe the underlying process in a simplified but unified mathematical language. This is also one of the major limitations of such effective descriptions. Many biological processes are intermittent, i.e., they switch between two or several phases. The most common examples are the run-and-tumble motion of bacteria [27–29] and foraging strategies of animals, e.g., predators who adopt hunting strategies by alternating between slow careful search and fast displacement (see Ref. [30] and references therein). In microbiology, examples include alternating phases of three-dimensional bulk diffusion and one-dimensional sliding along DNA chains of DNA-binding proteins [31–34], temporal trapping of tracers in polymer cages [35,36], binding and unbinding of macromolecules to form temporal ligand-receptor pairs or to neutralize pathogens by antibodies [37–42], switching between distinct conformational states [43,44], alternating phases of active and passive vesicle transport by motor proteins [45–49], alternating phases of bulk and surface diffusion [50–54], etc. The intermittent character of the motion makes the statistical analysis and biophysical interpretation of single particle trajectories even more challenging. If the intermittence is ignored, switching between several phases can be (mis)interpreted as a single effective phase with peculiar properties. For instance, switching between active (ballistic, $\alpha = 2$) and passive (diffusive, $\alpha = 1$) motion of a vesicle can be effectively understood as super-diffusion, with an intermediate scaling exponent $1 < \alpha < 2$. Moreover, intermittency can be also misleadingly interpreted as nonstationarity or nonergodicity of the process according to statistical tests. Identifying change points between distinct phases and their durations from a single trajectory is therefore an important

[*]yann.lanoiselee@polytechnique.edu
[†]Present address: International Joint Research Unit–UMI 2615 CNRS/ IUM/ IITP RAS/ Steklov MI RAS/ Skoltech/ HSE, Moscow, Russian Federation; denis.grebenkov@polytechnique.edu

statistical problem that can bring a finer, more accurate description of the underlying biological process.

Different statistical methods have been developed to detect change points of an intermittent stochastic process. Traditionally, Bayesian methods based on prior knowledge on the motion are preferred [55–61]. The prior knowledge is represented by the probability $P(\boldsymbol{x}_1,\ldots,\boldsymbol{x}_N|a_1,\ldots,a_K)$ of observing a trajectory $\boldsymbol{x}_1,\ldots,\boldsymbol{x}_N$ with N points, given the parameters $a_1,\ldots,a_K$ of the model. In other words, one defines a specific model-based functional of the trajectory to "process" the observed data. Once the model is chosen, its parameters $a_1,\ldots,a_K$ can be found by maximizing the likelihood of the observed trajectory according to the Bayesian rules. Although the Bayesian methods are statistically efficient, their practical implementation is rather time consuming, especially for long trajectories, while the results can be strongly biased by the choice of the underlying model made by researchers. In addition, when dealing with intermittent processes, one may need to probe many combinations of possible microscopic models for each phase. In this light, model-free methods can be preferred for the analysis of complex dynamics such as the intracellular transport.

In this paper, we address the challenging question of detection of change points between distinct phases in a single random trajectory without prior knowledge of the underlying stochastic model. The phases are distinguished by their dynamical properties such as different (i) diffusivities, (ii) drifts, (iii) auto-correlations of increments, (iv) distributions of increments, (v) dimensionalities (e.g., bulk/surface), (vi) isotropic/anisotropic character, or (vii) space accessibility (e.g., restricted character due to reflecting obstacles or confinement). The basic idea of such model-free methods consists in considering a *local* functional of the trajectory, $Q(n)$, which depends on a relatively small number of points around the point $\boldsymbol{x}_n$. When applied to successive points along the trajectory, this local functional transforms the trajectory into a new time series, which can then be used either to characterize the dynamics (e.g., to get local drift or diffusivity), or to discriminate between different phases of the motion. For instance, the points $\boldsymbol{x}_n$ with $Q(n)$ below some threshold can be assigned to one phase while the remaining points are assigned to the other phase. In contrast to Bayesian methods, the functional $Q(n)$, which is used to process the data, does not depend on the model, though the efficiency of this binary classification clearly depends on the choice of the functional $Q(n)$. The simplest choices,

$$Q_\mu(n) = \frac{1}{2\tau}(\boldsymbol{x}_{n+\tau} - \boldsymbol{x}_{n-\tau}), \tag{1}$$

$$Q_\sigma(n) = \frac{1}{2\tau+1}\sum_{k=-\tau}^{\tau} \|\boldsymbol{x}_{n+k+1} - \boldsymbol{x}_{n+k}\|^2, \tag{2}$$

are, respectively, the drift estimator and the variance estimator (over a window of size $2\tau+1$) of isotropic Brownian motion. Another standard functional is the angle between successive increments of the trajectory, which is often used to detect ballistic parts of the motion [49]. Having a differential form (i.e., involving differences between points), these functionals are rather sensitive to noise, exhibit large fluctuations and thus yield large statistical uncertainties. This drawback can be reduced by increasing the window size τ. However, too large τ would make the functional $Q(n)$ less sensitive to phase alternations, especially for short phases. Several improvements have been proposed, e.g., the root-mean-square estimator for the variance [62] or the scaling exponent extracted from the local TA MSD [47]. Nevertheless, these improved estimators still have the differential form and thus remain sensitive to noise.

To overcome this fundamental limitation, we propose the geometric properties of a *local convex hull* (LCH) as robust discriminators of different phases. In contrast to earlier used differential-like estimators, the convex hull is intrinsically an integral-like characteristic that is thus less sensitive to noise, as shown below. This new method is applicable for the analysis of single trajectories of any dimensionality. The method is model-free because it relies exclusively on geometric properties of the trajectory. We demonstrate its efficiency in recognizing different intermittent dynamical scenarios inspired from biology.

II. LOCAL CONVEX HULL METHOD

The convex hull of a finite set of points, $\{\boldsymbol{x}_1,\ldots,\boldsymbol{x}_n\} \subset \mathbb{R}^d$, is the set of all convex combinations based on these points:

$$\mathrm{Conv}(\boldsymbol{x}_1,\ldots,\boldsymbol{x}_n) = \left\{\sum_{k=1}^{n}\alpha_k\boldsymbol{x}_k | \alpha_k \geqslant 0, \sum_{k=1}^{n}\alpha_k = 1\right\}. \tag{3}$$

In simpler terms, it is the minimal convex shape that encloses all the points $\boldsymbol{x}_1,\ldots,\boldsymbol{x}_n$. In the planar case, the convex hull of a finite set of points $\{\boldsymbol{x}_1,\ldots,\boldsymbol{x}_n\}$ is a convex polygon whose vertices are some of the points in this set. The construction of a convex hull is thus reduced to identifying these points in a clockwise or counterclockwise order. In higher dimensions, the convex hull is a convex polytope (e.g., a convex polyhedron in three dimensions) whose vertices are some of the points in the input set. Among several efficient algorithms [63,64], we chose the quickhull algorithm [65] because of its available implementation in Matlab as functions "convhull" (in two dimensions) and "convhulln" (in higher dimensions). The convex hull has been used for home range estimations of animal territories [66–68] and for computation of fractal dimensions [69]. Some basic properties of the convex hull applied to stochastic processes are summarized in the Appendix.

We propose to consider the diameter and the volume of the local convex hull, computed over $2\tau+1$ trajectory points $\boldsymbol{x}_{n-\tau},\boldsymbol{x}_{n-\tau+1},\ldots,\boldsymbol{x}_{n+\tau}$, as two functionals:

$$Q_d(n) = \mathrm{diam}[\mathrm{Conv}(\boldsymbol{x}_{n-\tau},\ldots,\boldsymbol{x}_{n+\tau})], \tag{4}$$

$$Q_v(n) = \mathrm{vol}_d[\mathrm{Conv}(\boldsymbol{x}_{n-\tau},\ldots,\boldsymbol{x}_{n+\tau})] \tag{5}$$

(the volume is replaced by the area in two dimensions). Note that the diameter of the LCH is simply the largest distance between any two points in the sequence $\{\boldsymbol{x}_{n-\tau},\ldots,\boldsymbol{x}_{n+\tau}\}$, i.e., it is particularly easy to compute. Any significant change in the dynamics (i.e., switching between phases) is expected to be reflected in a notable change in the geometric form of the trajectory that is captured here by the local convex hull (Fig. 1). For instance, an increase in the diffusion coefficient or in the drift leads to larger increments and thus a larger LCH, with

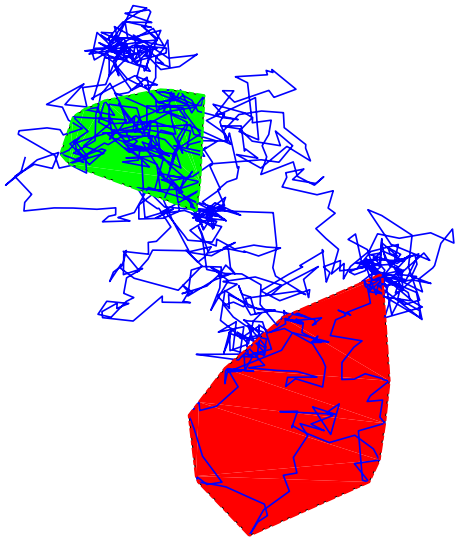

FIG. 1. Illustration of the local convex hull method applied to an intermittent planar trajectory, alternating a "fast" phase of Brownian motion (with $D = 1/2$) and a "slow" phase of an Ornstein-Uhlenbeck process (with $D = 1/2$ and $k = 0.1$; see Sec. III D), of equal durations $T_1 = T_2 = 40$. Only two LCHs (based on $2\tau + 1 = 41$ points) are shown by shadowed regions that correspond to the fast (dark red) and slow (light green) phases. Arbitrary units are used.

larger $Q_d(n)$ and $Q_v(n)$. In addition, anisotropic features of the motion, such as dimensionality reduction or presence of a reflecting wall, would be reflected in an anisotropic shape and in a reduced volume of the LCH. Depending on the observable chosen, the identification will be more sensitive to a particular aspect of the motion. The diameter is more sensitive to correlations and diffusion coefficients, whereas the volume is more sensitive to changes in the dimensionality and anisotropy. The window size τ is a parameter of the method that controls the compromise between reactivity and robustness in change points detection: smaller τ facilitates identification of short phases (the method is more reactive) but makes it less robust, as the estimators become more sensitive to fluctuations, noises, and outliers.

According to Eqs. (4) and (5), the point $\boldsymbol{x}_n$ contributes to $2\tau + 1$ estimators $Q_d(k)$ [or $Q_v(k)$] with $k \in [n - \tau, n + \tau]$. It is therefore natural to classify the point $\boldsymbol{x}_n$ by using all the estimators $Q_d(k)$ [or $Q_v(k)$], to which it contributed. We define thus the discriminator $S_d(n)$ as a weighted sum of $Q_d(k)$ over τ left and τ right neighbors of $\boldsymbol{x}_n$ [similar for $S_v(n)$]. The simplest choice consists in setting equal weights to each contribution:

$$S_d(n) = \frac{1}{2\tau + 1} \sum_{k=n-\tau}^{n+\tau} Q_d(k), \tag{6}$$

$$S_v(n) = \frac{1}{2\tau + 1} \sum_{k=n-\tau}^{n+\tau} Q_v(k). \tag{7}$$

Other weighting schemes (e.g., exponential) are as well possible.

The LCH method for change points detection consists in two steps. In the first step, for a given trajectory with N points, discriminators $S_d(n)$ and $S_v(n)$ are computed for all points $\boldsymbol{x}_n$ with n from $2\tau + 1$ to $N - 2\tau$ (the first and last 2τ points of the trajectory are discarded and remain unclassified). In other words, these discriminators transform the trajectory in $\mathbb{R}^d$ into two new one-dimensional time series. Due to the integral-like nature of the LCH, these times series are expected to be less erratic than trajectories and more sensitive to changes in the dynamics. In the second step, these time series are used to detect change points between two phases. In the basic setting, the points $\boldsymbol{x}_n$ with $S_d(n) > S_d$ (or $S_v(n) > S_v$) are classified as belonging to the "fast" phase whereas the points $\boldsymbol{x}_n$ with $S_d(n) \leqslant S_d$ (or $S_v(n) \leqslant S_v$) as belonging to the "slow" phase. The choice of the threshold value S_d (respectively, S_v) is crucial for an efficient detection of change points. Without *a priori* knowledge of the underlying stochastic process, we set S_d (respectively, S_v) to be the empirical mean of $S_d(n)$ [respectively, of $S_v(n)$] over the trajectory, i.e.,

$$S_d = \frac{1}{N - 4\tau} \sum_{n=2\tau+1}^{N-2\tau} S_d(n),$$

$$S_v = \frac{1}{N - 4\tau} \sum_{n=2\tau+1}^{N-2\tau} S_v(n). \tag{8}$$

In Sec. IV A, we discuss this point and possible improvements.

We emphasize that the LCH method can be applied to a *single* trajectory of essentially *any* intermittent stochastic process. In turn, the quality of change points detection depends on how distinct the geometric properties of two phases are, as well as on durations of these phases. We also stress that the method does not rely on specific properties of the underlying stochastic model, nor does it identify the properties of each phase. This analysis can be done by conventional methods after the change points detection. Finally, the same two phases do not need to be repeated along the trajectory. Although many distinct phases could in principle be present in a single trajectory, we focus on the particular case of two alternating phases (that we qualitatively called "fast" and "slow").

Note that the convex hull diameter can be considered as an alternative to the maximal excursion, i.e., the greatest distance from the origin that a particle reaches until time t [70]. The latter has been shown to have a narrower distribution than the conventional TA MSD and thus proposed as an estimator of the scaling exponent that can be applied to single particle trajectories [15].

III. NUMERICAL VALIDATION

In this section we investigate the efficiency of the LCH method by simulating six models of intermittent processes with the following phases:

(1) two planar Brownian motions with distinct diffusion coefficients D_1 and D_2 (change in diffusivity);

(2) two planar Brownian motions with the same diffusion coefficient D, with and without drift (change in directionality);

(3) two planar fractional Brownian motions with distinct Hurst exponents H_1 and H_2 (change in auto-correlations);

(4) planar Brownian motion and Ornstein-Uhlenbeck process (change in auto-correlations);

(5) planar Brownian motion and exponential flights (change in the distribution of increments);

(6) surface-mediated diffusion, with alternating phases of three-dimensional bulk diffusion and two-dimensional surface diffusion (change in dimensionality).

Although many other intermittent processes could be considered, we focus on the above cases as representative examples.

The simulations are performed as follows. First, we generate a thousand random trajectories, each with a thousand points (i.e., $N = 1000$). The intermittence is implemented by partitioning these points into two alternating phases by assigning random, exponentially distributed durations, with prescribed mean durations T_1 and T_2 of two phases. Throughout this section, we consider two phases of equal mean duration, $T_1 = T_2 = T$, while the situation of unequal phases is discussed in Sec. IV B. A white Gaussian noise of standard deviation σ_n is added to each trajectory point in order to check the robustness of the LCH method to measurement noises. The noise level σ_n is set to be proportional to the empirical standard deviation σ of increments, computed for each trajectory. Note that the noise has a stronger impact onto the "slow" phase than onto the "fast" phase. Second, we fix the window size τ and compute the diameter, $Q_d(n)$, and the volume, $Q_v(n)$, of the LCH at all time steps n from $\tau + 1$ to $N - \tau$ for each trajectory. These estimators are then transformed into the weighted discriminators $S_d(n)$ and $S_v(n)$ according to Eqs. (6) and (7) for n from $2\tau + 1$ to $N - 2\tau$. The default value of the window size τ is 10, other sizes being considered in Sec. IV A. Third, for each trajectory, we assign the points with $S_d(n) > S_d$ (respectively, $S_v(n) > S_v$) to the "fast" phase and the points with $S_d(n) \leqslant S_d$ (respectively, $S_v(n) \leqslant S_v$) to the "slow" phase, where S_d (respectively, S_v) is the empirical mean diameter (respectively, volume) of the LCH given by Eq. (8). We stress that the threshold value is computed separately for each trajectory. In this way, we obtain two *unrelated* binary classifications, the one based on the diameter and the other based on the volume. *A priori*, it is unclear which classification results in a better detection of change points. In practice, one would use one of these classifications, depending on the anticipated properties of the phases. Finally, to quantify the efficiency of the LCH method, we introduce the recognition score, R, as the fraction of points that have been correctly classified. This score is computed for each trajectory and then averaged over all simulated trajectories. The score 0.5 would be obtained by a completely random classification, whereas the score 1 corresponds to the perfect classification. We will analyze how the efficiency of the LCH method is affected by the phase duration T, the window size τ, and noise level σ_n. We emphasize that the phase classification is performed *individually* for each trajectory, whereas the ensemble average appears only at the last step to assess the quality of the method through the recognition score.

Throughout the paper, we employ dimensionless units. In particular, time is identified with the point index n.

A. Two Brownian motions

We start with heterogeneous diffusion, in which a particle diffuses in a composite medium with high and low diffusivities. A simplified model of this dynamics is a Brownian motion switching between two diffusion coefficients D_1 and D_2. This model can also represent the motion of a polymer that switches between two conformational states having distinct hydrodynamic radii (e.g., a compact globular structure versus an extended fibrous one).

Figure 2(a) shows a single planar trajectory with two alternating phases of slow ($D_1 = 1/2$) and fast ($D_2 = 2$) diffusion, each phase of the mean duration $T = 100$. The weighted LCH diameter $S_d(n)$ with the window size $\tau = 10$ is shown in Fig. 2(b). The change points are identified as crossings of $S_d(n)$ by the dashed horizontal line which indicates the empirical mean S_d over that trajectory. As expected, the detected change points are slightly delayed with respect to the actual change points (shown by changes of color/brightness in the curve). This delay is caused by the fact that the LCH at the actual change point, n_c, includes half points of one phase and half points of the other phase. Only when $n = n_c + 2\tau + 1$, the LCH gets rid off the points of the previous phase. As a consequence, the delay is expected to be of the order of 2τ, as qualitatively confirmed by this figure. The delay results in a false classification of some points, as illustrated by pink shadowed regions in Fig. 2(b). The false classification can also result from spontaneous crossings by $S_d(n)$ of the dashed horizontal line (e.g., see the shadowed region at the time step around 640). This is just random nature of the motion: the particle in the "fast" (respectively, "slow") phase starts to explore the space slower (respectively, faster) than usual due to stochastic fluctuations.

Figure 2(c) shows the recognition score R as a function of the mean phase duration T for the diameter-based discriminator $S_d(n)$. When the phase duration is too short (say, $T = 10$), the LCH of window size $\tau = 10$ includes 21 consecutive points and thus almost always contains points from both phases. In this extreme case, the method is clearly unable to detect change points, in agreement with the obtained recognition score close to 0.5. When the phase duration T is comparable to $2\tau + 1 = 21$ (the number of points used to construct the LCH) and two phases are quite distinct (the example $D_1 = 1/2$, $D_2 = 2$), the recognition score is around 0.67, i.e., two-thirds of points are correctly classified. The recognition score further increases up to 88% as the mean phase duration grows up to $T = 100$. If the delay in detection was equal on average to $c\tau$, the curve would be $(T - c\tau)/T = 1 - c\tau/T$, as illustrated by thin black line for $c = 1/2$. One can see that this hypothetical curve over-estimates the recognition score, probably because of additional spontaneous false classifications.

Figure 2(d) presents the recognition score for the volume-based classification. While this classification slightly outperforms the diameter-based one, the behavior is very similar to that shown in Fig. 2(c). This is not surprising because both phases and thus the shapes of the LCHs are isotropic so that the volume and the diameter of the LCH bear essentially the same information.

Figures 2(c) and 2(d) also show that the LCH estimators are robust against measurement noises. In fact, adding the white Gaussian noise of amplitude σ_n, which is comparable to the amplitude of one-step increments, has almost no effect on the recognition score. This is an important advantage of the LCH method, which is based on integral-like characteristics of the trajectory, as compared to conventional techniques based on differential-like estimators such as local TA MSD, which are

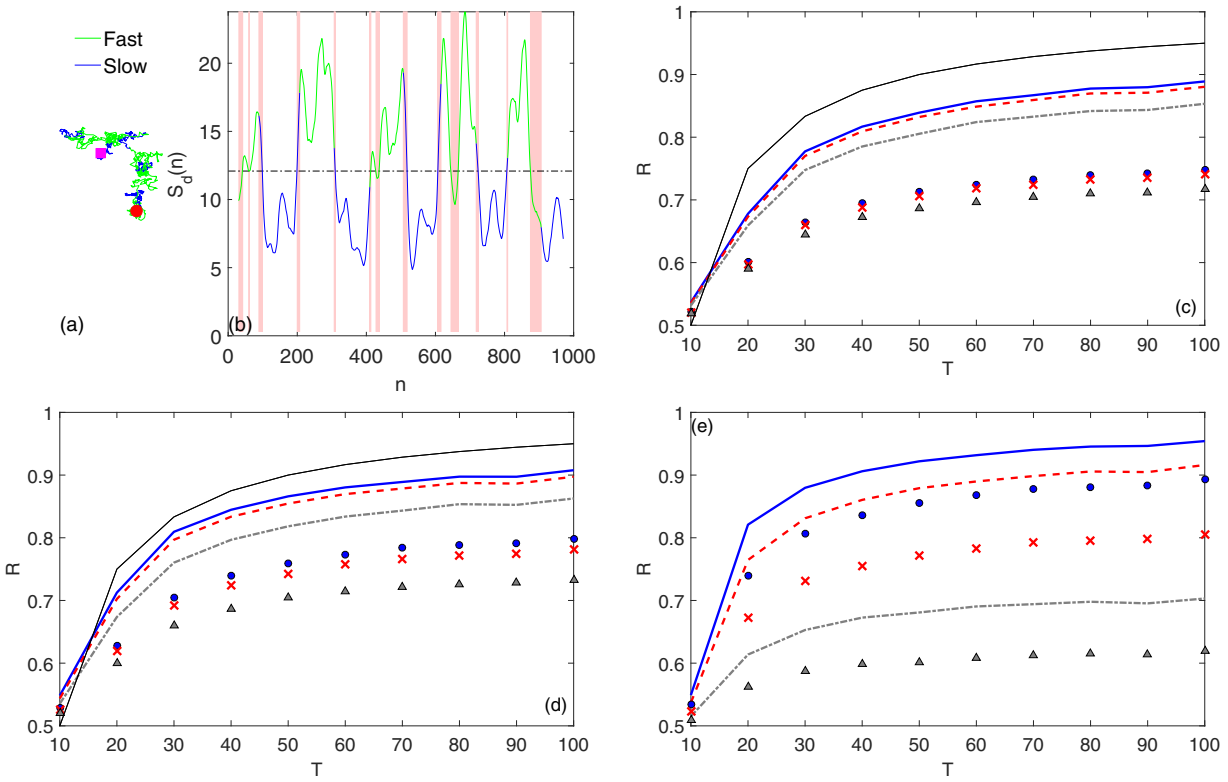

FIG. 2. Model 1. (a) A single trajectory of planar Brownian motion alternating a "slow" phase ($D_1 = 1/2$, dark blue) and a "fast" phase ($D_2 = 2$, light green), of the mean phase duration $T = 100$. Circle and square indicate the starting and ending points. (b) The weighted LCH diameter $S_d(n)$ with the window size $\tau = 10$, applied to this trajectory. Pink shadow highlights the false classification zones. Dashed horizontal line shows the empirical mean S_d over that trajectory. (c,d,e) Recognition score R of the diameter-based discriminator $S_d(n)$ (c), the volume-based discriminator $S_v(n)$ (d), and the TA MSD-based discriminator (e) as a function of the mean phase duration T. Lines show the results for the case $D_1 = 1/2$, $D_2 = 2$ with three noise levels σ_n: 0 (blue solid), 0.5σ (red dashed), and σ (gray dash-dotted) (σ being the empirical standard deviation of increment calculated for each trajectory). Symbols correspond to the case $D_1 = 1/2$, $D_2 = 1$ with the same levels of noise σ_n: 0 (circles), 0.5σ (crosses), and σ (triangles). Thin black solid line shows the hypothetical curve $1 - \tau/(2T)$ for qualitative comparison. Arbitrary units are used.

more sensitive to noise. This point is illustrated in Fig. 2(e), which shows the recognition score of the classification scheme, in which the LCH-based estimator $Q_d(n)$ is replaced by the local TA MSD estimator $Q_\sigma(n)$ from Eq. (2). We use the same window size $\tau = 10$ as for the LCH estimators. When there is no noise, the local TA MSD estimator outperforms the LCH-based estimators $Q_d(n)$ and $Q_v(n)$. This is not surprising as the diffusivity estimator $Q_\sigma(n)$ is known to be optimal for Brownian motion [62,71,72]. However, the presence of noise drastically deteriorates the quality of change points detection by TA MSD. In turn, the effect of the same level of noise onto the LCH-based estimator is much weaker.

When the diffusion coefficients of two phases become closer, the recognition score is reduced. This is illustrated in Figs. 2(c)–2(e) by symbols that show the recognition score for the case $D_1 = 1/2$ and $D_2 = 1$. In the ultimate case $D_1 = D_2$, the two phases become identical, and any phase detection is meaningless, yielding the recognition score close to 0.5 (not shown).

B. Brownian motion with a drift

In the second example, we consider a planar Brownian motion alternating two phases (of the same diffusivity), without and with a drift μ in a fixed direction. This is a very basic model for active intracellular transport, in which cargos can attach to motor proteins, be transported ballistically along microtubules, spontaneously detach, and resume diffusion [9,48]. If the intermittent character of this process was ignored, switching between two phases would effectively look like a superdiffusive motion with a scaling exponent α between 1 and 2.

As the drift tends to elongate the trajectory in one direction, one should be able to identify the drifted phase via anisotropic and larger LCH. To test the efficiency of the LCH method, we generate a planar Brownian motion alternating two phases, one of which has a small drift μ in a fixed direction. As previously, the durations of both phases are random and exponentially distributed variables with the mean phase duration T. Figure 3 shows an example of a single trajectory of this process, the weighted LCH diameter $S_d(n)$, and the recognition scores for the diameter-based and volume-based discriminators. For a relatively strong drift, $\mu = 0.5$ (with the one-step standard deviation $\sigma = 1$), both estimators efficiently detect the change points. For a much smaller drift $\mu = 0.1$, the recognition scores are decreased but remain good enough. For instance, one attains the recognition score of 80% at the mean phase duration $T = 100$. In both cases, the diameter-based

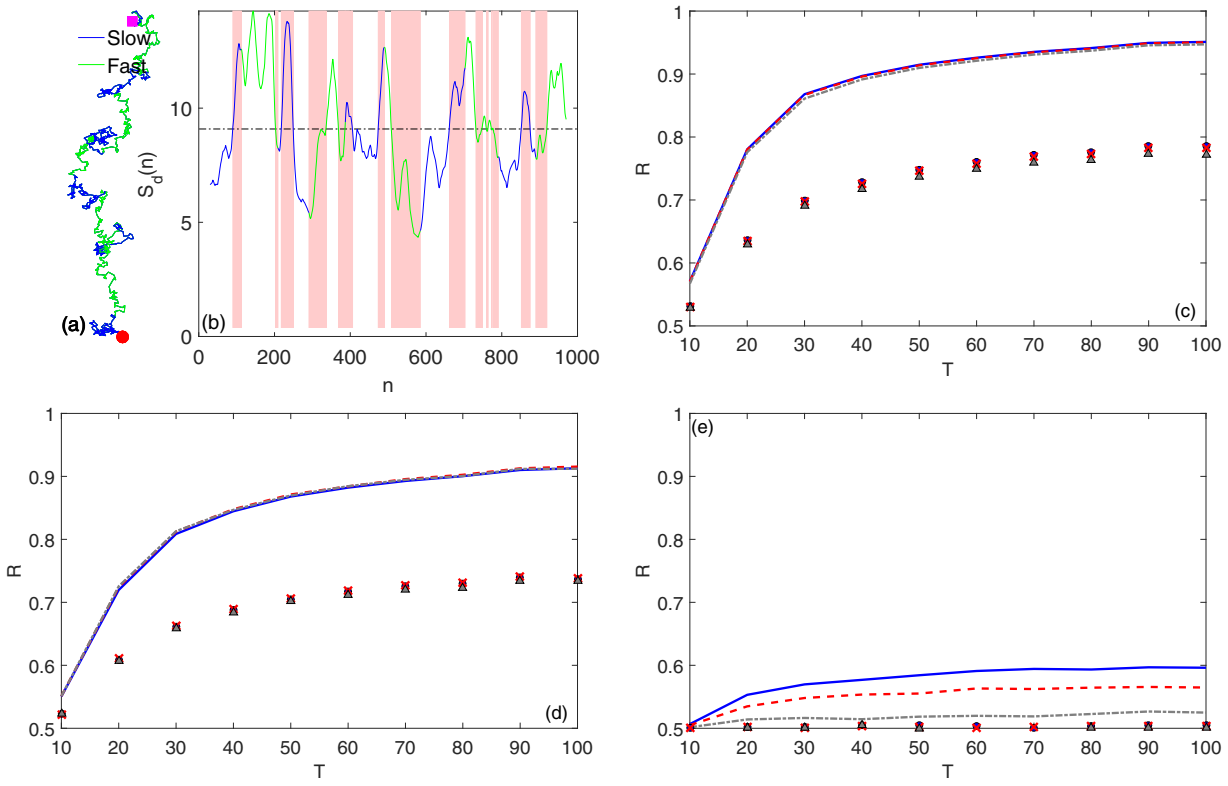

FIG. 3. Model 2. (a) A single trajectory of an intermittent process alternating a "slow" phase of planar Brownian motion without drift (dark blue) and a "fast" phase with drift ($\mu = 0.5$, light green), of the mean phase duration $T = 100$ (both phases with $D = 1/2$). Circle and square indicate the starting and ending points. (b) The weighted LCH diameter $S_d(n)$ with the window size $\tau = 10$ applied to this trajectory. Pink shadow highlights the false classification zones. Dashed horizontal line shows the empirical mean S_d over that trajectory. (c), (d), (e) Recognition score R of the diameter-based discriminator $S_d(n)$ (c), the volume-based discriminator $S_v(n)$ (d), and the TA MSD-based discriminator (e) as a function of the mean phase duration T. Lines show the results for the case $\mu = 0.5$ with three noise levels σ_n: 0 (blue solid), 0.5σ (red dashed), and σ (gray dash-dotted) (σ being the empirical standard deviation of increment calculated for each trajectory). Symbols correspond to the case $\mu = 0.1$ with the same levels of noise σ_n: 0 (circles), 0.5σ (crosses), and σ (triangles). Arbitrary units are used.

discriminator outperforms the volume-based discriminator, and both discriminators are very robust against noise. As expected, the local TA MSD estimator, which is *a priori* not adapted to detect drift, shows a poor performance [Fig. 3(e)].

C. Two fractional Brownian motions

The fractional Brownian motion $B_H(t)$ [73] is a centered Gaussian process, which is defined by its covariance function:

$$\langle B_H(t)B_H(s)\rangle = D_H[t^{2H} + s^{2H} - |t-s|^{2H}], \qquad (9)$$

where $0 < H < 1$ is the Hurst exponent, and D_H is the generalized diffusion coefficient. This is the long-range memory process that is often used to model antipersistent subdiffusive motion for $H < 1/2$ (e.g., the motion of a tracer in a viscoelastic medium with no characteristic timescale [4,8,74]) and persistent superdiffusive motion for $H > 1/2$ (e.g., active transport of cargos on microtubules by molecular motors [46–48,75]).

For each planar trajectory, X and Y coordinates were generated by concatenating independent "pieces" (phases) of one-dimensional fBm with alternating phases of subdiffusive ($H_1 = 0.35$) and superdiffusive ($H_2 = 0.7$) motion, with $D_H = 1/2$ in both cases. As previously, durations of phases are independent exponentially distributed random variables, with a prescribed mean phase duration T. In other words, the numerical algorithm consists in (i) generating a sequence of independent exponentially distributed durations $\tau_1, \tau_2, \ldots$, from which the integer change points are defined as $t_k = t_{k-1} + \lfloor \tau_k \rfloor$ (with $t_0 = 0$); and (ii) generating successive phases $\{x_{t_{k-1}+1}, \ldots, x_{t_k}\}$ and $\{y_{t_{k-1}+1}, \ldots, y_{t_k}\}$ (with $k = 1,2,\ldots$) as one-dimensional fBms, with the covariance defined in Eq. (9), where H is equal to H_1 for even k and to H_2 for odd k. The starting point of the "piece" k is the ending point of the "piece" $k-1$. The whole trajectory is thus composed of points

$$\Big\{ \underbrace{(x_1,y_1),\ldots,(x_{t_1},y_{t_1})}_{\text{"piece" 1: fast phase}}, \underbrace{(x_{t_1+1},y_{t_1+1}),\ldots,(x_{t_2},y_{t_2})}_{\text{"piece" 2: slow phase}},$$
$$\underbrace{(x_{t_2+1},y_{t_2+1}),\ldots,(x_{t_3},y_{t_3})}_{\text{"piece" 3: fast phase}},\ldots,$$
$$\ldots,\underbrace{(x_{t_K+1},y_{t_K+1}),\ldots,(x_N,y_N)}_{\text{"piece" K}} \Big\}.$$

Note that the last "piece" (with index K) is truncated to get the whole trajectory with N points. We emphasize that this algorithm yields the successive phases that are independent from each other, and there is no cross-correlation in increments

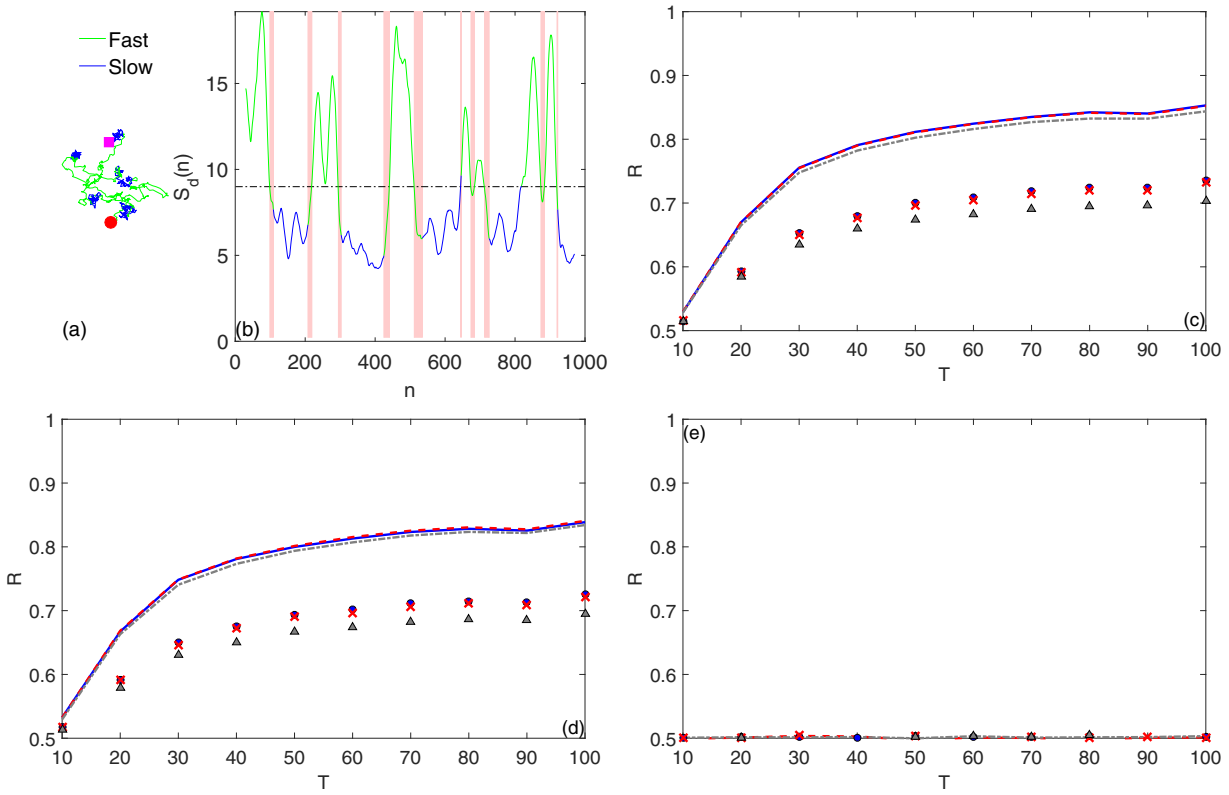

FIG. 4. Model 3. (a) A single trajectory of planar fBm, alternating a "slow" phase ($H_1 = 0.35$, dark blue) and a "fast" phase ($H_2 = 0.7$, light green), of the mean phase duration $T = 100$ and $D_H = 1/2$. Circle and square indicate the starting and ending points. (b) The weighted LCH diameter $S_d(n)$ with the window size $\tau = 10$ applied to this trajectory. Pink shadow highlights the false classification zones. Dashed horizontal line shows the empirical mean S_d over that trajectory. (c), (d), (e) Recognition score R of the diameter-based discriminator $S_d(n)$ (c), the volume-based discriminator $S_v(n)$ (d), and the TA MSD-based discriminator (e) as a function of the mean phase duration T. Lines show the results for the case $H_1 = 0.35$, $H_2 = 0.7$ with three noise levels σ_n: 0 (blue solid), 0.5σ (red dashed), and σ (gray dash-dotted) (σ being the empirical standard deviation of increment calculated for each trajectory). Symbols correspond to the case $H_1 = 0.35$, $H_2 = 0.5$ with the same levels of noise σ_n: 0 (circles), 0.5σ (crosses), and σ (triangles). Arbitrary units are used.

along X and Y coordinates. In this model, switching between two phases mimics changes in autocorrelations of increments.

Figure 4 shows an example of such intermittent trajectory, the weighted LCH diameter $S_d(n)$ with the window size $\tau = 10$ applied to this trajectory, and the recognition score for both the diameter-based and the volume-based classifications. The results are similar to that shown in Fig. 2 for intermittent Brownian motion. When the distinction between two phases is lower (the example with $H_1 = 0.35$ and $H_2 = 0.5$), the recognition scores are reduced (symbols) but remain satisfactory. These scores are particularly favorably compared to that of the TA MSD discriminator which cannot detect phases at all [Fig. 4(e)]. Although the conventional TA MSD estimator may be modified to show a better performance, such a modification would implicate additional knowledge on the model. The results for the case $H_1 = 0.5$ and $H_2 = 0.7$ (normal versus superdiffusive motion) are very similar to the latter case and thus not shown.

D. Brownian motion and Ornstein-Uhlenbeck process

The Ornstein-Uhlenbeck (OU) process is a Gaussian process modeling the diffusive motion of a particle trapped by a harmonic potential. This is a widely used model of particle interactions (e.g., a Rouse or bead-spring model in polymer physics [76,77]) and of the trapping effect of optical tweezers [8,74,78–80]. The one-dimensional OU process can be defined as a solution of the Langevin equation $dX_t = -kX_t dt + \sqrt{2D}dW_t$, where k is the relaxation rate (which is related to the spring constant), D is the diffusion coefficient, and W_t is the standard Brownian motion. For each planar trajectory, X and Y coordinates were generated as two independent intermittent processes, alternating a "fast" phase of Brownian motion ($k = 0$) and a "slow" phase of Ornstein-Uhlenbeck process ($k > 0$), with $D = 1/2$ for both phases. Phase durations were independent exponentially distributed random variables, with a prescribed mean phase duration T. This intermittent process can model the motion of a particle evolving in a medium where it freely moves until it interacts with an attracting trap, fluctuates near this trap via the OU process, liberates itself until the next interaction, etc. In neurosciences, the OU process is traditionally used as a model of the instantaneous firing rate of neurons in the neocortex [81,82]. Recently, a change-point detection procedure to detect changes in the spiking activity of neurons has been proposed [83]. In this section, we check the ability of the LCH method to detect the phases of motion governed by the OU process.

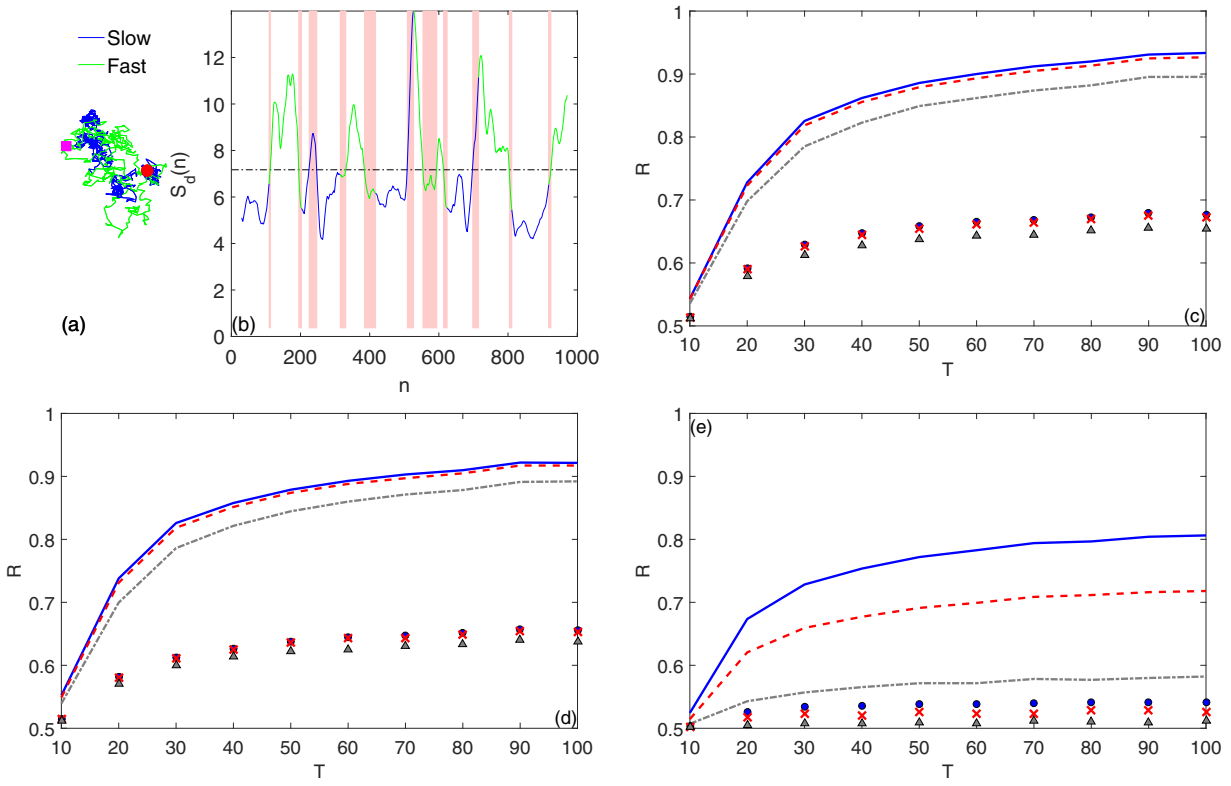

FIG. 5. Model 4. (a) A single trajectory of planar motion, alternating a "slow" phase ($k = 0.1$, dark blue) and a "fast" phase ($k = 0$, light green), with $D = 1/2$ and the mean phase duration $T = 100$. Circle and square indicate the starting and ending points. (b) The weighted LCH diameter $S_d(n)$ with the window size $\tau = 10$ applied to this trajectory. Pink shadow highlights the false classification zones. Dashed horizontal line shows the empirical mean S_d over that trajectory. (c), (d), (e) Recognition score R of the diameter-based discriminator $S_d(n)$ (c), the volume-based discriminator $S_v(n)$ (d), and the TA MSD-based discriminator (e) as a function of the mean phase duration T. Lines show the results for the case $k = 1$ with three noise levels σ_n: 0 (blue solid), 0.5σ (red dashed), and σ (gray dash-dotted) (σ being the empirical standard deviation of increment calculated for each trajectory). Symbols correspond to the case $k = 0.1$ with the same levels of noise σ_n: 0 (circles), 0.5σ (crosses), and σ (triangles). Arbitrary units are used.

Figure 5 shows an example of such intermittent trajectory, the weighted LCH diameter $S_d(n)$ with the window size $\tau = 10$ applied to this trajectory, and the recognition score for both the diameter-based and the volume-based classifications. The results are similar to that shown in Fig. 2 for intermittent Brownian motion. When k is getting smaller, the OU process becomes close to Brownian motion, and the recognition scores are reduced (symbols). The TA MSD discriminator shows poorer performance [Fig. 5(e)].

E. Brownian motion and exponential flights

To test the efficiency of the LCH method in detection of change points between phases with distinct distributions of increments, we consider an intermittent process, alternating a "slow" phase of planar Brownian motion (with $D = 1/2$) and a "fast" phase of two-dimensional exponential flights. In the "fast" phase, an increment at each time step was generated independently from the others as $(r\cos\theta, r\sin\theta)$, with the exponential distribution of flight length r (with the mean length ℓ) and the uniform distribution of angle θ. In other words, Gaussian increments (in the "slow" phase) are just replaced by such exponentially distributed increments (in the "fast" phase).

Figure 6 shows an example of such intermittent trajectory, the weighted LCH diameter $S_d(n)$ with the window size $\tau = 10$ applied to this trajectory, and the recognition score for both the diameter-based and the volume-based classifications. The results are similar to that shown in Fig. 2 for intermittent Brownian motion. The second choice of the mean flight length, $\ell = \sqrt{2}$, ensures that the variances of exponential flights and of Gaussian jumps are equal. In this case, two phases differ only in the distribution of increments (Gaussian versus exponential). Although these two distributions are relatively close (e.g., both distributions prohibit very large increments), the achieved classification is reasonably good. The performance of the TA MSD discriminator is comparable to that of the LCH for small noises but is reduced significantly for a larger noise.

We emphasize that our realization of exponential flights is different from the run-and-tumble model of bacteria motion, in which case a walker performs a ballistic motion for a random time and then undergoes random rotations [27,28]. We expect that the recognition score would be even higher for the run-and-tumble motion (as compared to our model) because two phases are geometrically more distinct.

F. Surface-mediated diffusion

In many biological and chemical applications, particles can adsorb to and desorb from the surface and thus alternate between bulk and surface diffusions. For instance, this so-called surface-mediated diffusion has been suggested as an

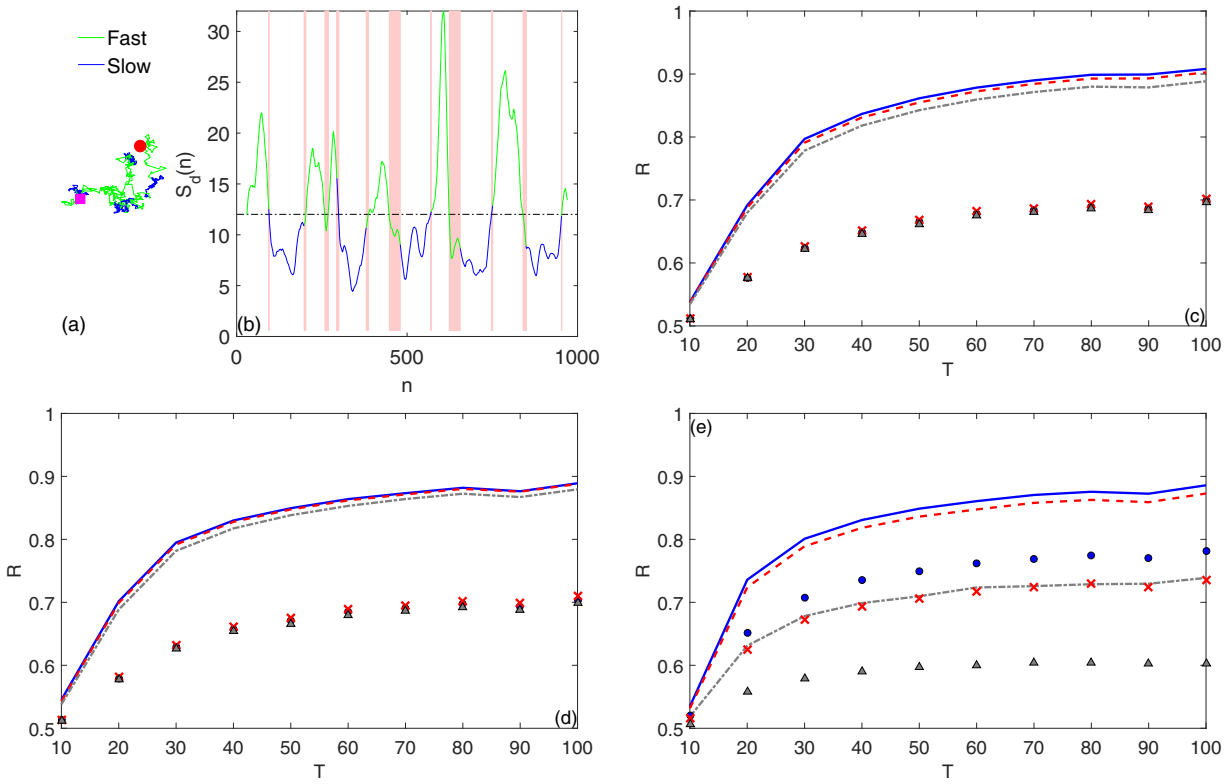

FIG. 6. Model 5. (a) A single trajectory of an intermittent process, alternating a "slow" phase of planar Brownian motion (with $D = 1/2$, dark blue) and a "fast" phase of two-dimensional exponential flights (with $\ell = 3$, light green), of the mean phase duration $T = 100$. Circle and square indicate the starting and ending points. (b) The weighted LCH diameter $S_d(n)$ with the window size $\tau = 10$ applied to this trajectory. Pink shadow highlights the false classification zones. Dashed horizontal line shows the empirical mean S_d over that trajectory. (c), (d), (e) Recognition score R of the diameter-based discriminator $S_d(n)$ (c), the volume-based discriminator $S_v(n)$ (d), and the TA MSD-based discriminator (e) as a function of the mean phase duration T. Lines show the results for the case $\ell = 3$ with three noise levels σ_n: 0 (blue solid), 0.5σ (red dashed), and σ (gray dash-dotted) (σ being the empirical standard deviation of increment calculated for each trajectory). Symbols correspond to the case $\ell = \sqrt{2}$ with the same levels of noise σ_n: 0 (circles), 0.5σ (crosses), and σ (triangles). Arbitrary units are used.

efficient search mechanism for DNA-binding proteins [31–34]. The statistics of durations of bulk and surface phases plays an important role, in particular, in predicting the mean first passage times [51–54]. For this reason, we test the LCH method on the surface-mediated diffusion inside a three-dimensional sphere of radius R. The particle starts from the origin of the sphere and undergoes Brownian motion in the bulk with diffusion coefficient D_{3d}, until the first arrival onto the surface. From this moment, the particle adsorbs to the surface and diffuses on the surface with the diffusion coefficient D_{2d}. The surface diffusion occurs during a random exponentially distributed waiting time (with the rate λ). After desorption, the particle is ejected into the bulk to the distance $a = 0.05R$ from the boundary and then resumes its bulk diffusion. Here we consider the equal diffusion coefficients $D_{2d} = D_{3d} = 10^{-3}$.

Figure 7 shows an example of such intermittent trajectory, the weighted LCH diameter $S_d(n)$ with the window size $\tau = 10$ applied to this trajectory, and the recognition score for both the diameter-based and the volume-based classifications. The significant difference of the surface-mediated diffusion as compared to the earlier considered models of intermittent processes is that the bulk phase duration is not an exponentially distributed random variable, it is determined by the statistics of first arrivals onto the surface. In turn, the duration of surface diffusion can be controlled by the desorption rate λ. Given that the mean surface duration is $1/\lambda$, we formally set $T = 1/\lambda$. This distinction explains new features in the recognition scores shown in Fig. 7(c) and 7(d). First, one can see that the volume-based discriminator greatly outperforms the diameter-based one. This is not surprising because the volume of the LCH is much more sensitive to the dimensionality reduction than the diameter. Second, in both cases, the recognition score does not grow monotonously with the mean phase duration T. In fact, the mean duration of the bulk phase, $[R^2 - (R - a)^2]/(6D)$, is fixed (and equal to 16.25 in our example), whereas the mean duration of the surface phase is progressively increased. As a consequence, as T grows, it becomes more difficult to detect the short bulk phases that results in the decrease of the recognition score. A similar behavior can be seen in Fig. 10 for intermittent Brownian motion (Model 1) when the durations of two phases differ significantly. Note also that the impact of noise is stronger than in other cases. The performance of the TA MSD discriminator is good but poorer than that of the volume-based estimator. This good performance is explained by the fact that the change in dimensionality from three dimensions to two dimensions also reduces the MSD from $6Dt$ and $4Dt$ that is captured by TA MSD estimator.

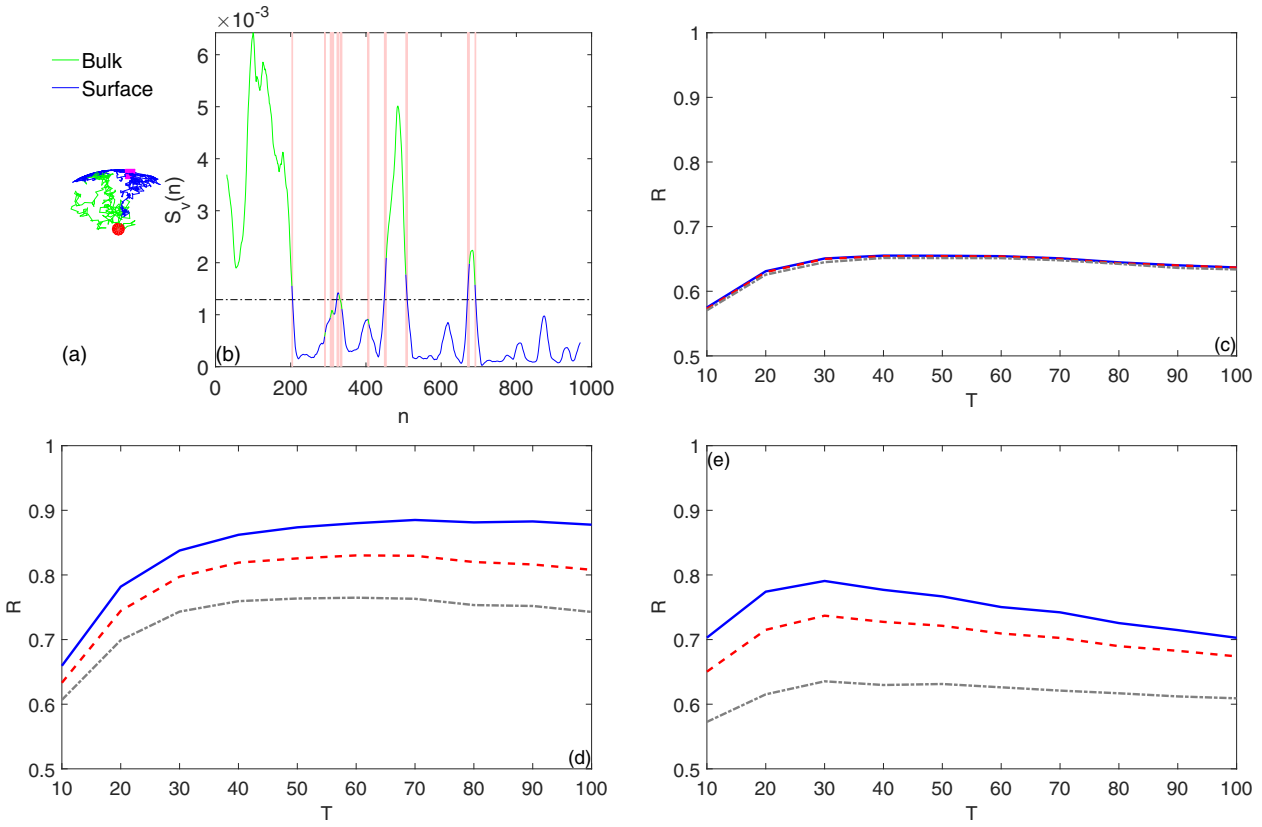

FIG. 7. Model 6. (a) A single trajectory of surface-mediated diffusion in a three-dimensional sphere of radius $R = 1$, alternating bulk diffusion (light green) and surface diffusion (dark blue), with $D_{2d} = D_{3d} = 10^{-3}$ and $\lambda = 10^{-2}$. Circle and square indicate the starting and ending points. (b) The weighted LCH diameter $S_d(n)$ with the window size $\tau = 10$ applied to this trajectory. Pink shadow highlights the false classification zones. Dashed horizontal line shows the empirical mean S_d over that trajectory. (c), (d), (e) Recognition score R of the diameter-based discriminator $S_d(n)$ (c), the volume-based discriminator $S_v(n)$ (d), and the TA MSD-based discriminator (e) as a function of the mean duration of the surface phase $T = 1/\lambda$. Three curves correspond to three noise levels σ_n: 0, 0.5σ, and σ (σ being the empirical standard deviation of increment calculated for each trajectory). Arbitrary units are used.

IV. DISCUSSION

The numerical validation has shown that the LCH method can detect change points between the phases that differ either by amplitudes of increments, or by the presence of drift, or by auto-correlations between increments, or by distribution of increments, or by dimensionality of the explored space. Moreover, the method is robust against noise due to the integral-like nature of the LCH-based estimators. In this section, we discuss the choice of the parameters, several limitations and future improvements of the method.

A. Parameters of the method

Although the LCH method is model-free, there are two parameters to be chosen: the window size τ and the threshold S_d (or S_v) used for the binary classification. Let us discuss the choice of these parameters in more detail.

Throughout Sec. III, we set $\tau = 10$. Figure 8 shows the effect of the window size τ on the recognition score R for intermittent Brownian motion (Model 1) with $D_1 = 1/2$, $D_2 = 2$, and the mean phase durations $T_1 = T_2 = 40$. First, one can see that the recognition score as a function of τ is not monotonous, i.e., there is an optimal window size τ_c that maximizes the recognition score. This optimality results from a compromise between the reactivity and the robustness of the method. In fact, the LCH contains too many points at large τ that leads to larger delays between actual and detected change points and thus increases the fraction of false classifications. In turn, when τ is too small, the method is reactive (delays are short) but also too sensitive to stochastic fluctuations within one phase; as a consequence, the fraction of false classifications is also higher due to spontaneous crossings of the discriminator $S_d(n)$ [or $S_v(n)$] of the mean level S_d (or S_v). This latter effect is drastically enhanced in the presence of noise (see how the curves with larger noise levels σ_n are diminished at short τ). As a consequence, the optimal window size τ_c is increased for noisier data. Clearly, the τ_c should also depend on the phase duration. One cannot therefore choose the optimal window size without *a priori* knowledge about the noise and phase durations. In practice, the range $5 \leqslant \tau \leqslant 10$ seems to be the reasonable choice of the window size. Note that the recognition score versus τ for the intermittent fBm (Model 3) exhibits very similar behavior (not shown).

The second parameter of the method is the threshold S_d (or S_v) that is used to distinguish "slow" and "fast" phases. Without prior knowledge about the process, we chose the arithmetic mean of the discriminator $S_d(n)$ [or $S_v(n)$] over

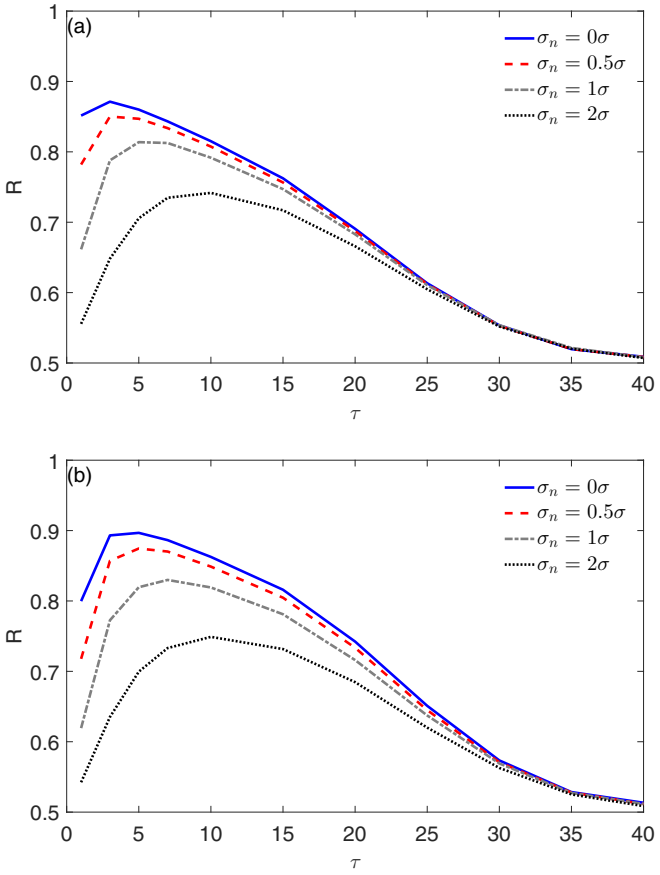

FIG. 8. Effect of the window size τ on the recognition score R for intermittent Brownian motion (Model 1) with $D_1 = 1/2$, $D_2 = 2$, and the mean phase durations $T_1 = T_2 = 40$. (a) The diameter-based discriminator $S_d(n)$; (b) the volume-based discriminator $S_v(n)$. Four curves correspond to four noise levels σ_n: 0, 0.5σ, σ, and 2σ (σ being the empirical standard deviation of increment calculated for each trajectory). Arbitrary units are used.

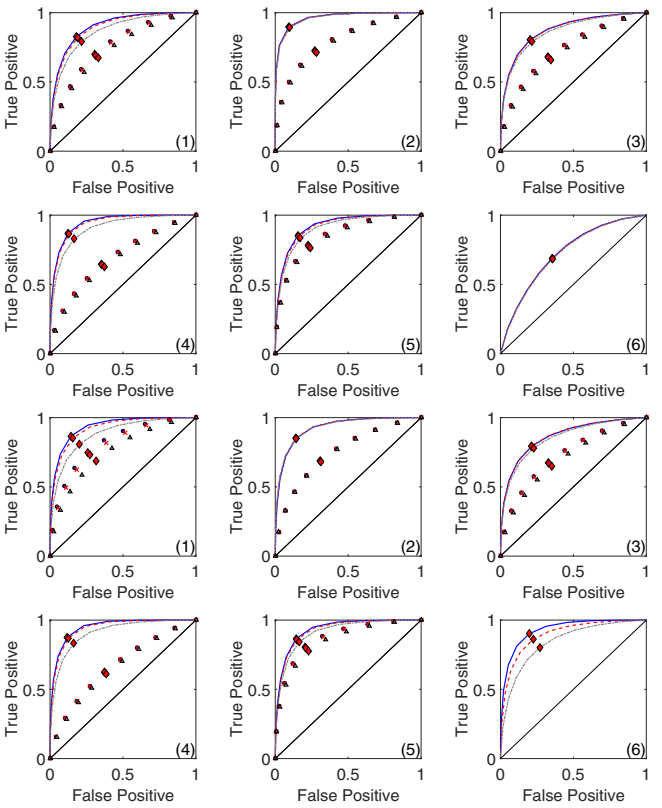

FIG. 9. Effect of the threshold on the recognition quality for six models (following the enumeration at the beginning of Sec. III), for the diameter-based discriminator (top 6 plots) and the volume-based discriminator (bottom 6 plots). The left lower corner and the right upper corner correspond to the threshold at the maximal and the minimal values, whereas diamonds indicate the mean value S_d (or S_v) used as the threshold throughout the paper. Legend of six curves on each plot is the same as in Figs. 2–7 for the recognition score (three levels of noise and two sets of model parameters, except for the Model 6).

the trajectory as the threshold. However, this choice is not necessarily optimal. For instance, one could use another mean (e.g., quadratic or harmonic), or set the threshold to be proportional to the mean, or choose another function or constant. In order to justify this empirical choice, we consider a receiver operating characteristic (ROC) curve for both diameter-based and volume-based discriminators. For this purpose, we compute the true positive rate (the fraction of "fast" phase points that were identified as "fast") and the false-positive rate (the fraction of "slow" phase points that were identified as "fast") by varying the threshold from the minimal to the maximal value of the discriminator $S_d(n)$ [or $S_v(n)$]. Figure 9 shows the ROC curves for six considered models and for two discriminators at the mean duration time $T = 40$. An ideal discriminator would yield the true positive rate at 1 and the false-positive rate at 0 (the left upper corner), whereas a random discriminator would fill the diagonal. The threshold at the minimal value of the discriminator classifies all points as belonging to the "fast" phase (as $S_d(n) \geqslant \min_n\{S_d(n)\}$) that corresponds to the right upper corner. Similarly, the threshold at the maximal value of the discriminator classifies all points as belonging to the "slow" phase (as $S_d(n) \leqslant \max_n\{S_d(n)\}$) that corresponds to the left lower corner. The intermediate thresholds yield a concave ROC curve lying above the diagonal. The diamond symbols indicate the threshold at the mean value S_d (or S_v) that we suggest and use in this paper. One can see that this value is the closest to the left upper corner and thus the optimal choice, at least for the considered models and sets of parameters.

The choice of the threshold is related to another important question about the choice of the LCH-based geometric property as the discriminator. The local convex hull captures changes in the mutual arrangment of points, in a somewhat similar way as our eyes do. The diameter and the volume are the basic geometric characteristics of the LCH that reflect, respectively, the overall size and anisotropy of points. Although these characteristics appear to be natural, one can use any function of these (or other) characteristics as well. It is still unclear what is the optimal function of the local convex hull to distinguish between two phases. In other words, among all possible functions of the LCH, which one would yield the highest recognition score. We expect that the optimal

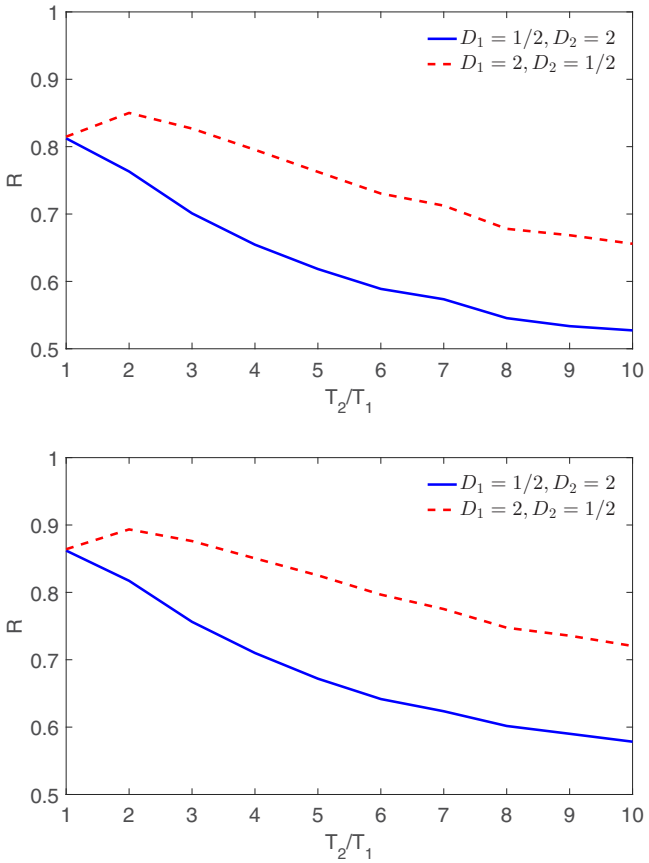

FIG. 10. Effect of unequal phase durations for planar Brownian motion alternating "slow" and "fast" phases (Model 1). Recognition score R of the diameter-based discriminator $S_d(n)$ (a) and the volume-based discriminator $S_v(n)$ (b) as a function of the second phase duration T_2 while the first phase duration T_1 is kept fixed: $T_1 = 40$. Solid line: the first phase is "slow" ($D_1 = 1/2$), the second phase is "fast" ($D_2 = 2$); dashes line: the first phase is "fast" ($D_1 = 2$), the second phase is "slow" ($D_2 = 1/2$). Arbitrary units are used.

choice that maximizes the recognition score, depends on the stochastic model of both phases.

B. Phase durations

In all examples studied in Sec. III (except for surface-mediated diffusion), phase durations were chosen as independent exponentially distributed random variables with equal mean phase durations: $T_1 = T_2 = T$. This means that all phases have distinct but similar durations, whose average and standard deviation are equal to T.

When two phases have significantly different durations, the detection of the shorter phase can be problematic. To illustrate this point, we consider again the intermittent Brownian motion (Model 1), in which one phase duration is kept fixed, whereas the other phase duration is variable (in contrast to earlier figures, here the phase durations are fixed, not exponentially distributed). Figure 10 shows the recognition score as a function of T_2/T_1, with fixed $T_1 = 40$. Solid line corresponds to the case, in which the first phase is "slow" and the second phase is "fast." As the duration of the fast phase increases, its points start to dominate in the geometric properties of the LCH, and thus to shift the threshold S_d (or S_v) to higher values. As a consequence, the detection of shorter slow phases becomes more difficult, and the recognition score decreases. In the opposite case, when the first phase is "fast" and the second phase is "slow" (dashed line), the situation is slightly different. One can see that the recognition score first increases and then decreases. We conclude that short "slow" phases are on average more difficult to detect than short "fast" phases. In both cases, the method is incapable of detecting the phases shorter than or comparable to the window size τ, which in turn should not be smaller than 5–10 steps.

If we assume that there are no phases shorter than some T_0 (≈10–20), any shorter phase detected by the algorithm can be attributed to a spontaneous crossing of $S_d(n)$ [or $S_v(n)$] of the mean level. The recognition quality can thus be improved by reclassifying such inappropriate phases. For instance, if a too short slow phase is detected between two fast phases, the slow phase can be reclassified into the fast one, i.e., these three consecutive phases are merged and classified as a single fast phase. This post-processing correction is particularly important when one aims at getting the statistics of slow and fast phase durations. In fact, a spurious short slow phase of the above example cut a long fast phase into two shorter pieces and thus significantly affected the statistics of phase durations. For a better performance, such post-processing corrections or more elaborate statistical techniques (such as an estimation of likelihood of short phases) need to be elaborated and tested on an application-specific basis. Note also that even if the corrected short phase was not spurious (and thus the correction was erroneous), the correction may still improve the overall recognition score, as it eliminates two false classifications related to the delays. We emphasize that this correction procedure has not been used in this paper.

V. CONCLUSION

We introduced a new model-free local convex hull method for detecting change points in a single-particle trajectory. The LCH is constructed on a small number of consecutive points of the trajectory and thus reflects the dynamics *locally*. In this way, the trajectory is transformed into two time series, the diameter and the volume of the LCH along the trajectory. These time series are then used for a binary classification into "slow" and "fast" phases.

The LCH method was validated on six common models of intermittent processes: Brownian motion with two diffusivities, Brownian motion with and without drift, fractional Brownian motion with different Hurst exponents, Brownian motion with and without harmonic potential, Brownian motion and exponential flights, and surface-mediated diffusion. For all these models, we computed the recognition score R as the fraction of successfully classified points. We showed that R grows with the mean phase duration and reaches the values as high as 90% at $T = 100$ when two phases were quite distinct. We analyzed how distinct two phases should be for a robust classification. We also showed that, due to the integral-like character of the LCH, the method is much more robust against noise than conventional methods such as, e.g., time averaged mean square displacement. In particular, the TA MSD discriminator has outperformed the LCH discriminators

only in the case of two alternating Brownian motions and only without noise. In all other cases, the performance of LCH estimators was much higher. The LCH method, being based on purely geometric features of the trajectory, can be applied to a wide range of relevant intermittent processes such as animal foraging, active/passive motion in the cell or motion exhibiting a change in dimensionality. The LCH method also has the potential to be successfully applied to detect changes in instantaneous firing rates in neurons.

ACKNOWLEDGMENT

D.G. acknowledges the support under Grant No. ANR-13-JSV5-0006-01 of the French National Research Agency.

APPENDIX: SOME PROPERTIES OF THE CONVEX HULL

The convex hull of points of a random trajectory is a highly nontrivial geometric functional of this trajectory. Here we summarize several rigorous results for both Brownian motion and simple random walk.

Takacs showed that the mean perimeter of the convex hull of standard Brownian motion W_t in the plane is

$$\mathbb{E}\{\mathrm{vol}_1[\mathrm{Conv}(W_t)]\} = \sqrt{16\pi Dt}, \tag{A1}$$

whereas El Bahir obtained the mean area [84,85]

$$\mathbb{E}\{\mathrm{vol}_2[\mathrm{Conv}(W_t)]\} = \pi Dt. \tag{A2}$$

More general results for a standard Brownian motion W_t in $\mathbb{R}^d$ read [86]

$$\mathbb{E}\{\mathrm{vol}_d[\mathrm{Conv}(W_t)]\} = \frac{(\pi Dt)^{d/2}}{\Gamma(d/2+1)^2}, \tag{A3}$$

$$\mathbb{E}\{\mathrm{vol}_{d-1}[\mathrm{Conv}(W_t)]\} = \frac{2(4\pi Dt)^{(d-1)/2}}{\Gamma(d)}. \tag{A4}$$

Extensions to a set of n Brownian paths have been provided in Ref. [85]. The perimeter of the planar convex hull in the case of confinement to a semi-infinite domain presents nontrivial behavior as a function of distance from the starting point to the boundary [87].

These formulas are exact for continuous Brownian motion. However, experimental trajectories are discretized so that Eqs. (A3) and (A4) can only be valid asymptotically when the number of points in the convex hull is large. In turn, our LCH estimators are based on a relatively small number of points, and Eqs. (A3) and (A4) are thus not applicable. Spitzer and Widom considered a two-dimensional discrete random walk, modeled as a sum of independent random variables in the complex plane, and derived the average perimeter of the related convex hull [88],

$$\langle L_N \rangle = 2\sum_{k=1}^{N} \frac{\mathbb{E}(|x_k + iy_k|)}{k} \tag{A5}$$

(here $x_k + iy_k$ is the position of the walker in the complex plane after k steps), with the concentration inequality [91]

$$\mathbb{P}\{|L_N - \langle L_N \rangle| \geqslant \varepsilon\} \leqslant 2\exp\left(-\frac{\varepsilon^2}{8\pi^2 N}\right). \tag{A6}$$

Some other properties were reported in Ref. [91]. The asymptotic behavior of the mean perimeter and the mean area of the convex hull over planar random walks was investigated in Ref. [89]. The obtained formulas are even applicable to a moderate number of jumps that makes them suitable for the analysis of the local convex hulls. The distributions of the area and of the perimeter of the convex hull were computed numerically by a sophisticated large-deviation approach in Ref. [90]. The properties of the convex hull of Gaussian samples and of d-dimensional fractional Brownian motion were analyzed in Refs. [92,93].

[1] I. M. Tolić-Nørrelykke, E.-L. Munteanu, G. Thon, L. Oddershede, and K. Berg-Sørensen, Anomalous Diffusion in Living Yeast Cells, Phys. Rev. Lett. **93**, 078102 (2004).
[2] I. Golding and E. C. Cox, Physical Nature of Bacterial Cytoplasm, Phys. Rev. Lett. **96**, 098102 (2006).
[3] C. Wilhelm, Out-of-Equilibrium Microrheology inside Living Cells, Phys. Rev. Lett. **101**, 028101 (2008).
[4] J. Szymanski and M. Weiss, Elucidating the Origin of Anomalous Diffusion in Crowded Fluids, Phys. Rev. Lett. **103**, 038102 (2009).
[5] R. Metzler, V. Tejedor, J.-H. Jeon, Y. He, W. H. Deng, S. Burov, and E. Barkai, Analysis of single particle trajectories: From normal to anomalous diffusion, Acta Phys. Pol. B **40**, 1315 (2009).
[6] E. Sackmann, F. Keber, and D. Heinrich, Physics of cellular movements, Ann. Rev. Conden. Matt. Phys. **1**, 257 (2010).
[7] J.-H. Jeon, V. Tejedor, S. Burov, E. Barkai, C. Selhuber-Unkel, K. Berg-Sørensen, L. Oddershede, and R. Metzler, *In Vivo* Anomalous Diffusion and Weak Ergodicity Breaking of Lipid Granules, Phys. Rev. Lett. **106**, 048103 (2011).
[8] E. Bertseva, D. S. Grebenkov, P. Schmidhauser, S. Gribkova, S. Jeney, and L. Forró, Optical trapping microrheology in cultured human cells, Eur. Phys. J. E **35**, 63 (2012).
[9] P. C. Bressloff and J. M. Newby, Stochastic models of intracellular transport, Rev. Mod. Phys. **85**, 135 (2013).
[10] N. Gal, D. Lechtman-Goldstein, and D. Weihs, Particle tracking in living cells: A review of the mean square displacement method and beyond, Rheol. Acta **52**, 425 (2013).
[11] R. Metzler, J.-H. Jeon, A. Cherstvy, and E. Barkai, Anomalous diffusion models and their properties: non-stationarity, non-ergodicity, and ageing at the centenary of single particle tracking, Phys. Chem. Chem. Phys. **16**, 24128 (2014).
[12] E. Kepten, A. Weron, G. Sikora, K. Burnecki, and Y. Garini, Guidelines for the fitting of anomalous diffusion mean square displacement graphs from single particle tracking experiments, PLoS ONE **10**, e0117722 (2015).
[13] S. Condamin, V. Tejedor, R. Voituriez, O. Bénichou, and J. Klafter, Probing microscopic origins of confined subdiffusion by first-passage observables, Proc. Natl. Acad. Sci. USA **105**, 5675 (2008).

[14] D. A. Kenwright, A. W. Harrison, T. A. Waigh, P. G. Woodman, and V. J. Allan, First-passage-probability analysis of active transport in live cells, Phys. Rev. E **86**, 031910 (2012).
[15] V. Tejedor, O. Bénichou, R. Voituriez, R. Jungmann, F. Simmel, C. Selhuber-unkel, L. B. Oddershede, and R. Metzler, Quantitative analysis of single particle trajectories: Mean maximal excursion method, Biophys. J. **98**, 1364 (2010).
[16] F. Thiel, F. Flegel, and I. M. Sokolov, Disentangling Sources of Anomalous Diffusion, Phys. Rev. Lett. **111**, 010601 (2013).
[17] Y. Meroz, I. M. Sokolov, and J. Klafter, Test for Determining a Subdiffusive Model in Ergodic Systems from Single Trajectories, Phys. Rev. Lett. **110**, 090601 (2013).
[18] Y. Meroz and I. M. Sokolov, A toolbox for determining subdiffusive mechanisms, Phys. Rep. **573**, 1 (2015).
[19] K. Burnecki, E. Kepten, J. Janczura, I. Bronshtein, Y. Garini, and A. Weron, Universal algorithm for identification of fractional Brownian motion. A case of telomere subdiffusion, Biophys. J. **103**, 1839 (2012).
[20] M. Magdziarz, A. Weron, K. Burnecki, and J. Klafter, Fractional Brownian Motion Versus the Continuous-Time Random Walk: A Simple Test for Subdiffusive Dynamics, Phys. Rev. Lett. **103**, 180602 (2009).
[21] M. Weiss, Single-particle tracking data reveal anticorrelated fractional Brownian motion in crowded fluids, Phys. Rev. E **88**, 010101 (2013).
[22] D. Ernst, J. Köhler, and M. Weiss, Probing the type of anomalous diffusion with single-particle tracking, Phys. Chem. Chem. Phys. **16**, 7686 (2014).
[23] M. Magdziarz and A. Weron, Anomalous diffusion: Testing ergodicity breaking in experimental data, Phys. Rev E **84**, 051138 (2011).
[24] Y. Lanoiselée and D. S. Grebenkov, Revealing nonergodic dynamics in living cells from a single particle trajectory, Phys. Rev. E **93**, 052146 (2016).
[25] B. Chen and Y. Hong, Testing for the markov property in time series, Eco. Theo. **28**, 130 (2012).
[26] O. Bénichou and R. Voituriez, From first-passage times of random walks in confinement to geometry-controlled kinetics, Phys. Rep. **539**, 225 (2014).
[27] H. C. Berg and D. A. Brown, Chemotaxis in *Escherichia coli* analysed by three-dimensional tracking, Nature **239**, 500 (1972).
[28] H. C. Berg, *E. coli in Motion* (Springer-Verlag, New York, 2004).
[29] J. Tailleur and M. E. Cates, Statistical Mechanics of Interacting Run-and-Tumble Bacteria, Phys. Rev. Lett. **100**, 218103 (2008).
[30] O. Bénichou, C. Loverdo, M. Moreau, and R. Voituriez, Intermittent search strategies, Rev. Mod. Phys. **83**, 81 (2011).
[31] P. H. Richter and M. Eigen, Diffusion controlled reaction rates in spheroidal geometry: Application to repressor-operator association and membrane bound enzymes, Biophys. Chem. **2**, 255 (1974).
[32] O. G. Berg, R. B. Winter, and P. H. von Hippel, Diffusion-driven mechanisms of protein translocation on nucleic acids. 1. Models and theory, Biochemistry **20**, 6929 (1981).
[33] P. H. von Hippel and O. G. Berg, Facilitated target location in biological systems, J. Biol. Chem. **264**, 675 (1989).
[34] C. Loverdo, O. Bénichou, R. Voituriez, A. Biebricher, I. Bonnet, and P. Desbiolles, Quantifying Hopping and Jumping in Facilitated Diffusion of DNA-Binding Proteins, Phys. Rev. Lett. **102**, 188101 (2009).
[35] I. Y. Wong, M. L. Gardel, D. R. Reichman, E. R. Weeks, M. T. Valentine, A. R. Bausch, and D. A. Weitz, Anomalous Diffusion Probes Microstructure Dynamics of Entangled F-Actin Networks, Phys. Rev. Lett. **92**, 178101 (2004).
[36] E. Fodor, H. Hayakawa, P. Visco, and F. van Wijland, Active cage model of glassy dynamics, Phys. Rev. E **94**, 012610 (2016).
[37] D. Shoup and A. Szabo, Role of diffusion in ligand binding to macromolecules and cell-bound receptors, Biophys. J. **40**, 33 (1982).
[38] R. Zwanzig and A. Szabo, Time dependent rate of diffusion-influenced ligand binding to receptors on cell surfaces, Biophys. J. **60**, 671 (1991).
[39] M. J. Saxton, Anomalous diffusion due to binding: A Monte Carlo study, Biophys. J. **70**, 1250 (1996).
[40] P. Bongrand, Ligand-receptor interactions, Rep. Prog. Phys. **62**, 921 (1999).
[41] A. Michelman-Ribeiro, D. Mazza, T. Rosales, T. J. Stasevich, H. Boukari, V. Rishi, C. Vinson, J. R. Knutson, and J. G. McNally, Direct measurement of association and dissociation rates of DNA binding in live cells, Biophys. J. **97**, 337 (2009).
[42] J. A. Torreno-Pina, B. M. Castro, C. Manzo, S. I. Buschow, A. Cambi, and M. F. Garcia-Parajo, Enhanced receptor-clathrin interactions induced by *N*-glycan-mediated membrane micropatterning, Proc. Natl. Acad. Sci. USA **111**, 11037 (2014).
[43] C. Calderon, Detection of subtle dynamical changes induced by unresolved "conformational coordinates" in single-molecule trajectories via goodness-of-fit tests, J. Phys. Chem. B **114**, 3242 (2010).
[44] M. Galanti, D. Fanelli, and F. Piazza, Conformation-controlled binding kinetics of antibodies, Sci. Rep. **6**, 18976 (2016).
[45] M. Saxton, Single-particle tracking: Models of directed transport, Biophys. J. **67**, 2110 (1994).
[46] A. Caspi, R. Granek, and M. Elbaum, Enhanced Diffusion in Active Intracellular Transport, Phys. Rev. Lett. **85**, 5655 (2000).
[47] D. Arcizet, B. Meier, E. Sackmann, J. O. Rädler, and D. Heinrich, Temporal Analysis of Active and Passive Transport in Living Cells, Phys. Rev. Lett. **101**, 248103 (2008).
[48] C. P. Brangwynne, G. H. Koenderink, F. C. MacKintosh, and D. A. Weitz, Intracellular transport by active diffusion, Trends Cell Biol. **19**, 423 (2009).
[49] E. A. Katrukha, M. Mikhaylova, H. X. van Brakel, P. M. van Bergen en Henegouwen, A. Akhmanova, C. C. Hoogenraad, and L. C. Kapitein, Probing cytoskeletal modulation of passive and active intracellular dynamics using nanobody-functionalized quantum dots, Nat. Commun. **8**, 14772 (2017).
[50] P. Levitz, Random flights in confining interfacial systems, J. Phys. Condens. Matter **17**, S4059 (2005).
[51] O. Bénichou, D. S. Grebenkov, P. Levitz, C. Loverdo, and R. Voituriez, Optimal Reaction Time for Surface-Mediated Diffusion, Phys. Rev. Lett. **105**, 150606 (2010).
[52] O. Bénichou, D. S. Grebenkov, P. Levitz, C. Loverdo, and R. Voituriez, Mean first-passage time of surface-mediated diffusion in spherical domains, J. Stat. Phys. **142**, 657 (2011).
[53] J.-F. Rupprecht, O. Bénichou, D. S. Grebenkov, and R. Voituriez, Kinetics of active surface-mediated diffusion in spherically symmetric domains, J. Stat. Phys. **147**, 891 (2012).
[54] F. Rojo, C. E. Budde, Jr., H. S. Wio, and C. E. Budde, Enhanced transport through desorption-mediated diffusion, Phys. Rev. E **87**, 012115 (2013).

[55] R. P. Adams and D. J. C. MacKay, Bayesian online changepoint detection, arXiv:0710.3742.
[56] D. Barber, A. T. Cemgil, and S. Chiappa, *Bayesian Time Series Models* (Cambridge University Press, Cambridge, 2011), pp. 1–26.
[57] S. Türkcan and J.-B. Masson, Bayesian decision tree for the classification of the mode of motion in single-molecule trajectories, PloS ONE **8**, e82799 (2013).
[58] J.-B. Masson, P. Dionne, C. Salvatico, M. Renner, C. G. Specht, A. Triller, and M. Dahan, Mapping the energy and diffusion landscapes of membrane proteins at the cell surface using high-density single-molecule imaging and Bayesian inference: Application to the multiscale dynamics of glycine receptors in the neuronal membrane, Biophys. J. **106**, 74 (2014).
[59] P. J. Bosch, J. S. Kanger, and V. Subramaniam, Classification of dynamical diffusion states in single molecule tracking microscopy, Biophys. J. **107**, 588 (2014).
[60] E. Ruggieri and M. Antonellis, An exact approach to Bayesian sequential change point detection, Comput. Stat. Data Anal. **97**, 71 (2016).
[61] K. Hinsen and G. R. Kneller, Communication: A multiscale Bayesian inference approach to analyzing subdiffusion in particle trajectories, J. Chem. Phys. **145**, 151101 (2016).
[62] D. S. Grebenkov, Time-averaged quadratic functionals of a Gaussian process, Phys. Rev. E **83**, 061117 (2011).
[63] J. O'Rourke, *Computational Geometry in C*, 2nd ed., Cambridge Tracts in Theoretical Computer Science (Cambridge University Press, Cambridge, 1998).
[64] M. de Berg, O. Cheong, M. van Kreveld, and M. Overmars, *Computational Geometry: Algorithms and Applications*, 3rd ed. (Springer-Verlag, Berlin-Heidelberg, 2008).
[65] C. B. Barber, D. P. Dobkin, and H. T. Huhdanpaa, The quickhull algorithm for convex hulls, ACM Trans. Math. Software **22**, 469 (1996).
[66] B. J. Worton, A convex hull based estimator of homerange size, Biometrics **51**, 1206 (1995).
[67] W. M. Getz and C. C. Wilmers, A local nearest neighbor convex-hull construction of home ranges and utilization distribution, Ecography **27**, 489 (2004).
[68] J. Randon-Furling, S. N. Majumdar, and A. Comtet, Convex Hull of N planar Brownian Motions: Exact Results and an Application to Ecology, Phys. Rev. Lett. **103**, 140602 (2009).
[69] F. Normant and C. Tricot, Method for evaluating the fractal dimension of curves using convex hulls, Phys. Rev. A **43**, 6518 (1991).
[70] R. Bidaux, J. Chave, and R. Vocka, Finite time and asymptotic behavior of the maximal excursion of a random walk, J. Phys. A: Math. Gen. **32**, 5009 (1999).
[71] G. Voisinne, A. Alexandrou, and J.-B. Masson, Quantifying biomolecule diffusivity using an optimal Bayesian method, Biophys. J. **98**, 596 (2010).
[72] A. J. Berglund, Statistics of camera-based single-particle tracking, Phys. Rev. E **82**, 011917 (2010).
[73] B. B. Mandelbrot and J. W. Van Ness, Fractional Brownian motions, fractional noises and applications, SIAM Rev. **10**, 422 (1968).
[74] D. S. Grebenkov, M. Vahabi, E. Bertseva, L. Forro, and S. Jeney, Hydrodynamic and subdiffusive motion of tracers in a viscoelastic medium, Phys. Rev. E **88**, 040701(R) (2013).
[75] M. A. Desposito, C. Pallavicini, V. Levi, and L. Bruno, Active transport in complex media: Relationship between persistence and superdiffusion, Physica A **390**, 1026 (2011).
[76] M. Doi and S. F. Edwards, *The Theory of Polymer Dynamics* (Clarendon Press, London, 1986).
[77] P.-G. de Gennes, *Introduction to Polymer Dynamics* (Cambridge University Press, Cambridge, 1990).
[78] S. C. Kuo and M. P. Sheetz, Force of single kinesin molecules measured with optical tweezers, Science **260**, 232 (1993).
[79] D. Wirtz, Particle-tracking microrheology of living cells: Principles and applications, Ann. Rev. Biophys. **38**, 301 (2009).
[80] D. S. Grebenkov, First exit times of harmonically trapped particles: A didactic review, J. Phys. A **48**, 013001 (2015).
[81] D. J. Amit and N. Brunel, Model of global spontaneous activity and local structured activity during delay periods in the cerebral cortex, Cereb Cortex. **7**, 237 (1997).
[82] D. J. Amit and N. Brunel, Dynamics of a recurrent network of spiking neurons before and following learning, Network: Comput. Neural Syst. **8**, 373 (1997).
[83] L. Mazzucato, A. Fontanini, and G. La Camera, Dynamics of multistable states during ongoing and evoked cortical activity, J. Neurosci. **35**, 8214 (2015).
[84] L. Takács, Expected perimeter length, Amer. Math. Month. **87**, 5 (1980).
[85] S. N. Majumdar, A. Comtet, and J. Randon-Furling, Random convex hulls and extreme value statistics, J. Stat. Phys. **138**, 995 (2010).
[86] R. Eldan, Volumetric properties of the convex hull of an n-dimensional Brownian motion, Elec. Jour. Prob. **19**, 1 (2014).
[87] M. Chupeau, O. Bénichou, and S. N. Majumdar, Convex hull of a Brownian motion in confinement, Phys. Rev. E **91**, 050104 (2015).
[88] F. Spitzer and H. Widom, The circumference of a convex polygon, Proc. Amer. Math. Soc. **12**, 506 (1961).
[89] D. S. Grebenkov, Y. Lanoiselée, and S. N. Majumdar, Mean perimeter and mean area of the convex hull over planar random walks, arXiv:1706.08052.
[90] G. Claussen, A. K. Hartmann, and S. N. Majumdar, Convex hulls of random walks: Large-deviation properties, Phys. Rev. E **91**, 052104 (2015).
[91] T. L. Snyder and J. M. Steele, Convex hulls of random walks, Proc. Am. Math. Soc. **117**, 1165 (1993).
[92] Y. Davydov, On convex hull of Gaussian samples, Lit. Math. Jour. **51**, 171 (2011).
[93] Y. Davydov, On convex hull of d-dimensional fractional Brownian motion, Stat. Prob. Let. **82**, 37 (2012).